V International Conference on Particle-based Methods – Fundamentals and Applications
PARTICLES 2017
P. Wriggers, M. Bischoff, E. Oñate, D.R.J. Owen, & T. Zohdi (Eds)

INSTABILITIES OF A SAND LAYER SUBJECTED TO AN UPWARD WATER FLOW BY A 2D COUPLED DISCRETE ELEMENT - LATTICE BOLTZMANN HYDROMECHANICAL MODEL

MOULOUD MANSOURI[1], MOULAY S. EL YOUSSOUFI [2,3] AND FRANÇOIS NICOT[4]

[1] Département de Génie Civil, Université Ferhat Abbas Setif 1
19000, Setif, Algeria
email : mansouri.mouloud@univ-setif.dz

[2] LMGC - UMR 5508, Université de Montpellier - CC048
163 rue Auguste Broussonnet, 34090 Montpellier, France
[3] Laboratoire de Micromécanique et d'Intgrité des Structures (MIST)
IRSN-CNRS-Université de Montpellier, France
email : moulay-said.el-youssoufi@umontpellier.fr

[4] Université Grenoble-Alpes, IRSTEA, Unité de Recherche ETNA
Domaine Universitaire, BP 76, F38402 - Saint Martin d'Hères, France
email : francois.nicot@irstea.fr

Key words: Discrete Element Method, Lattice Boltzmann, quicksand

Abstract. This work deals with the numerical simulation of the instabilities occurring in a sand layer subjected to an upward water flow. A coupled Discrete Elements - Lattice Boltzmann hydromechanical model is used for this end. After a brief presentation of the numerical model, simulations of an upward fluid flow through granular deposits are performed for two cases namely under controlled hydraulic gradients and under controlled volumetric flow rates. In the first case i.e. under controlled hydraulic gradient, the simulations show that the quicksand condition is actually reached for a hydraulic gradient very close to the critical hydraulic gradient calculated from the global analysis of classical soil mechanics. The simulations point out moreover that the quicksand phenomenon could be produced locally under slightly lower gradients. In the second case i.e. under controlled volumetric flow rates, the simulations show that there are three levels of flow ; low flow rates that allow infiltration without any destabilization, medium flow rates that cause expansion of the deposit to increase its permeability and high flow rates which may cause the formation continuous tunnel between the upstream and the downstream sides as well as sand boils. It is shown also that under the controlled flow rate condition the hydraulic gradient remains in all cases less than the average critical hydraulic gradient.

1 INTRODUCTION

Quicksand condition can occur for a layer of sand subjected to an upward flow under a hydraulic gradient close to the critical hydraulic gradient. The latter corresponds to the state where the seepage force equals the submerged weight of the sand layer. Even if the classical soil mechanics allows to obtain the critical hydraulic gradient which defines the state of the beginning of soil uplift, it is not able to show the evolution of a soil layer subjected to upward flow before and after the quicksand condition is reached. Furthermore, it does not allow to define the size of the zone affected by the phenomenon, i.e. a restricted zone or a generalized uplift.

This work presents an analysis of the evolution of a sand layer subjected to an upward flow under two different conditions ; first under a gradually increased hydraulic gradient and second under a gradually increased volumetric flow rate. The analysis is carried out using a numerical model based on the coupling of a discrete method to model the sand grains with the Lattice Boltzmann method to model the water flow [1]. For the sake of simplicity, the analysis is carried using 2D simulations.

2 DISCRETE ELEMENT METHOD

The Discrete Element approach models the grains of a granular material by independent elements, each element interacts with its neighbors at the contact points. The overall deformation of the medium is mainly due to the relative movements of the grains assumed as rigid bodies. Therefore, the behavior of the medium can be described through the integration of the dynamic equations applied to each element. Such equations are written through Newton's second law by taking all external forces into account, such as the contact forces, the gravitational forces and the hydrodynamic forces. Since these forces can change abruptly with time, the integration should be performed in an incremental manner using small time steps.

The mollecular dynamics method originally proposed by Cundall and Strack [2] is implemented in this work. This method allows a slight overlap of the grains which is used to calculate the contact forces through explicit lows. We deal in this work with a 2D modeling where the grains are assumed circular, hence to detect the contacts at each time step the normal distance between any two grains i and j is examined. This distance is computed as : $D_n = \|\vec{x}_j - \vec{x}_i\| - r_j - r_i$, where $\vec{x}_i$, $\vec{x}_j$ are the i and j grains positions and r_i, r_j their radii respectively. The two grains are in contact if they overlap ($D_n \leq 0$). A contact force applied by a grain j on a grain i is decomposed into normal and tangential components. The normal force is calculated here using the viscoelastic linear model (Fig.1a), hence $\vec{F}_n = (-k_n D_n - \nu_n V_n).\vec{n}$, where V_n is the normal velocity of the grain j relative to the grain i, k_n and ν_n are the elastic and the viscous damping constants respectively and $\vec{n}$ is the unit vector pointing from i to j, i.e. : $\vec{n} = (\vec{x}_j - \vec{x}_i)/\|\vec{x}_j - \vec{x}_i\|$.

The tangential force is computed using the viscoelastic - frictional model (Fig.1b) as $\vec{F}_s = min\left(k_s D_s + \nu_s V_s, \mu F_n\right)\vec{s}$, where $\vec{s}$ is the tangential unit vector obtained by rota-

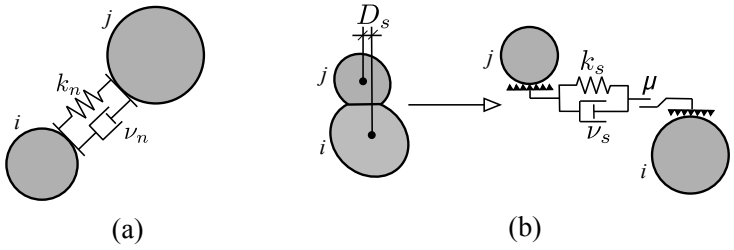

Figure 1: Modeling of the contact interaction forces ; (a) the normal force model, (b) the tagential force model.

tion of the normal vector $\vec{n}$ by an angle $\pi/2$ in the counterclockwise direction, V_s is the tangential velocity of the grain j relative to the grain i, D_s is the cumulative tangential displacement of the grain j relative to the grain i from the moment of contact initiation, μ is the Coulomb's coefficient of friction, k_s and ν_s are the tangential elastic and viscous damping constants respectively.

It should be noted that the choice of the elastic and the viscous damping constants (k_n and ν_n) is not arbitrary, in fact k_n must be high enough to avoid substantial overlap that affects the overall behavior, whereas ν_n that controls the damping in the material is selected such that the restitution coefficient ϵ_n defined as the ratio of the normal velocities at the start and the end of the contact is between 0 and 1.

Once the contact forces and the other external forces acting on a grain are obtained at a discrete time t, accelerations are calculated through the dynamic equations,then integrated to obtain the kinematic variables of the grain at time $(t + \Delta t)$. Considering that accelerations are not constant during a time increment Δt, special algorithms are used to predict accurately the kinematic variables, such as the Velocity-Verlet algorithm.

Finally, it is important to note that in order to correctly describe the evolution of the contact force, the time step Δt should be sufficiently small compared to the contact duration t_c. It is usually taken as $\Delta t \approx t_c/10$. For the viscoelastic model the contact duration can be approximated by $t_c = \pi\sqrt{m_{eff}/k_n}$, where $m_{eff} = m_i m_j/(m_i + m_j)$, m_i and m_j are the masses of the grains in contact. Therefore the maximum time step is computed as :

$$\Delta t_{max} \approx 0.1\pi\sqrt{m/k_n} \tag{1}$$

where m is the smallest effective mass in the system.

3 LATTICE BOLTZMANN METHOD

In the Lattice Boltzmann Method, one solves the kinetic equation for the particle distribution function $f(\vec{x}, \vec{\xi}, t)$, which depends on the spatial position $\vec{x}$, the velocity of particules $\vec{\xi}$, at the time t. The macroscopic quantities of interest such as mass density ρ and momentum density $\rho\vec{u}$ are weighted averages of the distribution function :

$$\rho = \int f d\vec{\xi} \qquad \text{(a)} \qquad\qquad \rho\vec{u} = \int \vec{\xi} f d\vec{\xi} \qquad \text{(b)} \tag{2}$$

A popular kinetic model adopted for the method is the so-called BGK (Bhatnagar, Gross and Krook) model. In this model the collisions term in the Boltzmann equation is simplified using the simple relaxation time approximation :

$$\frac{\partial f}{\partial t} + \vec{\xi}.\vec{\nabla} f = -\frac{1}{\lambda}(f - f^{(0)}) \tag{3}$$

where $f^{(0)}$ is the equilibrium distribution function (Maxwell-Boltzmann equilibrium function) and λ is the relaxation time. To solve for f numerically, Eq.(3) is discretized twice : a first discretization with respect to the time involving a time increment Δt and a second discretization based on the velocity space by chosing a finite set of velocity vectors that particles can have. The continuous particle distribution function $f(\vec{x}, \vec{\xi}, t)$ becomes therefore, a set of discrete distributions $f_i(\vec{x}, t)$ associated with the chosen velocity vectors $\vec{e}_i$. As an illustration, here is presented the D2Q9 model (2 Dimensions, 9 Velocity vectors) which is widely used for 2D simulations. Figure 2a, sketches the discrete velocity vectors in the D2Q9 model.

The discretizations lead to the LBGK (Lattice BGK) equation, that describes the incremental evolution of the discrete particle distributions f_i :

$$f_i(\vec{x} + \vec{e}_i \Delta t, t + \Delta t) - f_i(\vec{x}, t) = -\frac{1}{\tau}\left(f_i(\vec{x}, t) - f_i^{(eq)}(\vec{x}, t)\right) \tag{4}$$

where $f_i^{(eq)}$ is the discrete equilibrium distribution given as :

$$f_i^{(eq)} = \rho w_i \left[1 + \frac{3}{c^2}\vec{e}_i.\vec{u} + \frac{9}{2c^4}(\vec{e}_i.\vec{u})^2 - \frac{3}{2c^2}\vec{u}.\vec{u}\right] \tag{5}$$

where c is a characteristic speed of the model, w_i being the weighting factors; $w_0 = 4/9$, $w_{2,4,6,8} = 1/9$, $w_{1,3,5,7} = 1/36$, τ is the dimensionless relaxation time such as $\frac{1}{\tau} = \frac{\Delta t}{\lambda}$.

Equation (4) describes the incremental evolution of the discrete particle distributions f_i at the nodes of a regular lattice having a space step $\Delta x = c\Delta t$ (Fig. 2b). Hence if the space discretization's step is selected, the characteristic speed of the model is defined by $c = \frac{\Delta x}{\Delta t}$.

The fluid pressure p can be computed from the mass density through the equation of state $p = c_s^2 \rho$, where c_s is the sound speed of the model related to the lattice model's speed c as $c_s = c/\sqrt{3}$.

It is shown through the Chapman-Enskog analysis [3] that LB models recover the incompressible Navier-Stokes equations when the density fluctuation of the fluid is assumed to be negligible and the equivalent kinematic viscosity is given by :

$$\nu = \frac{1}{3}c\Delta x\left(\tau - \frac{1}{2}\right) \tag{6}$$

Therefore, in order to correctly simulate an incompressible fluid flow, one must ensure that the density fluctuation is sufficiently small. This can be achieved using a model with

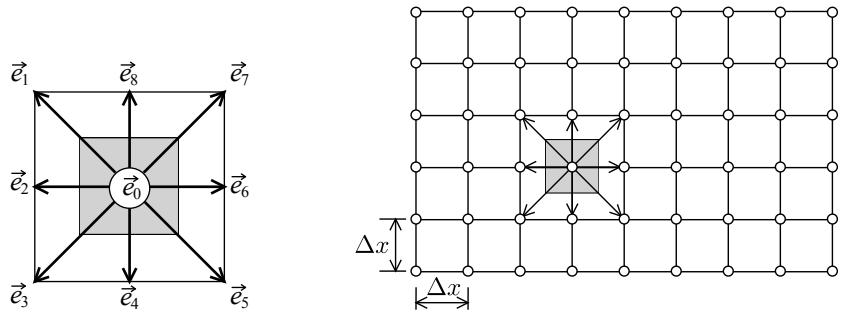

Figure 2: (a) D2Q9 model, (b) Flow domain discretization using the D2Q9 model

the sound speed c_s is larger enough than the maximum velocity of the simulated flow u_{max}, i.e. with a 'computational' Mach number defined as $M_a = \frac{u_{max}}{c_s}$ sufficiently small. In practice, M_a should be maintained, smaller than 0.1.

The discretization parameters are Δx, Δt and τ, if the viscosity of the fluid is given, only two of these parameters can be chosen independently since they are related through Eq. 6. In practice, it is often convenient to choose τ and Δx as two independent parameters and compute Δt from Eq. 6. This is due to the fact that τ is largely responsible for the numerical stability of LB simulations and Δx is often dictated by the space description precision. In practice τ is typically chosen in the range $]0.5\,,\,3]$.

4 COUPLED DISCRETE ELEMENT - LATTICE BOLTZMANN MODEL

4.1 Solid moving boundary treatment and hydrodynamic forces computation

The treatment of a solid moving boundary is decisive in granular materials hydromechanics. To model the fluid-solid no slip condition, we use in this work the interpolated bounce back scheme proposed by Bouzidi et al. [4]. For a linear interpolation, the post-collision distributions to be assigned to the solid boundary nodes before the streaming step are

$$\begin{cases} f_{\hat{i}}^{out}(\vec{x}_s,t) = 2q f_i^{out}(\vec{x}_f,t) + (1-2q) f_i^{out}(\vec{x}_{f'},t) + 6 w_i \rho_w \frac{\vec{e}_{\hat{i}}.\vec{u}_w}{c^2}, & q \leqslant \frac{1}{2} \\ f_{\hat{i}}^{out}(\vec{x}_s,t) = \frac{1}{2q} f_i^{out}(\vec{x}_f,t) + \frac{2q-1}{2q} f_{\hat{i}}^{out}(\vec{x}_{f'},t) + \frac{3}{q} w_i \rho_w \frac{\vec{e}_{\hat{i}}.\vec{u}_w}{c^2}, & q \geqslant \frac{1}{2} \end{cases} \tag{7}$$

where $\vec{e}_{\hat{i}}$ refers to the opposite direction of the direction $\vec{e}_i$ ($\vec{e}_{\hat{i}} = -\vec{e}_i$), $\vec{u}_w$ is the velocity of the boundary, ρ_w is the fluid mass density at the boundary and q defines the fraction of the boundary intersected link located in the fluid domain and calculated by referring to Figure 3 as $q = \frac{\|\vec{x}_f - \vec{x}_w\|}{\|\vec{x}_f - \vec{x}_s\|}$.

When a solid boundary moves, there are grid nodes that move from the solid region into the fluid region to become fluid nodes (indicated by □ in Fig. 3). Therefore one must specify the distribution functions applying to these nodes. In this work, unknown distri-

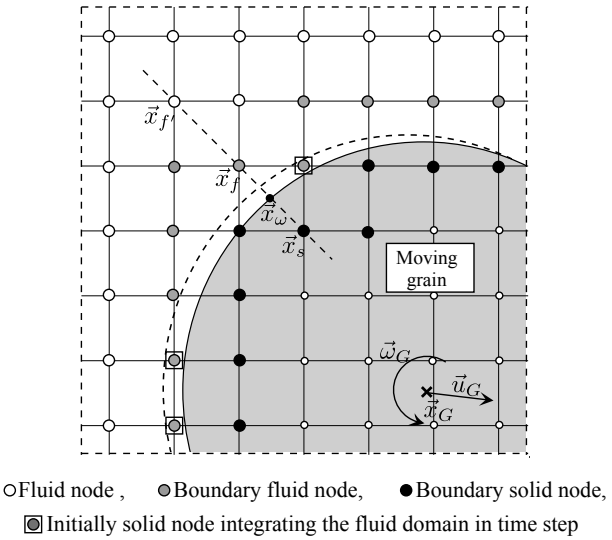

Figure 3: Representation of a moving grain on the lattice grid

butions are approximated as the equilibrium distributions computed using the averaged fluid's density in the whole system and the velocity of the solid particle at the specified node's position just before it leaves the solid region.

The hydrodynamic forces are computed in this work through the momentum exchange method [3].

4.2 Coupling procedure

As mentioned in the previous section, the time step in LBM (noted in the following Δt_{LB}) depends on the other discretization parameters and calculated from Eq. 6. Δt_{LB} is often larger than the maximum value DEM time step noted here Δt_{DEmax} and calculated from Eq. 1. Therfore, one should perform a number n_d of DEM computation steps then perform one LB computation step. This can be carried out by selecting the DEM time step $\Delta t_{DE} \leqslant \Delta t_{DEmax}$, such that $n_d \Delta t_{DE} = \Delta t_{LB}$, with the integer number n_d may be computed as $n_d = Int\left(\frac{\Delta t_{LB}}{\Delta t_{DEmax}}\right) + 1$, then the DEM time step is set :

$$\Delta t_{DE} = \frac{\Delta t_{LB}}{n_d} \tag{8}$$

Note finally that the static buoyancy force is taken into account by multiplying the gravitationnal acceleration by the coefficient $(1 - \rho_w/\rho_s)$, where ρ_w and ρ_s are the fluid and solid densities respectively.

5 2D SIMULATIONS OF AN UPWARD WATER FLOW THROUGH A SAND LAYER

It is worth noting that 2D discrete element modeling of a granular deposit produces a porous model with non interconnected pores. This completely changes the hydraulic properties of a saturated granular material. Therefore, the grains are maintained spaced, so that intergranular pores remain interconnected. The radii of grains are slightly increased in the discrete element modeling while kept equal to the actual radii in the Lattice-Boltzmann discretization. Thus the contact forces between the grains develop before the contact actually occurs. In this study, the distance added to the actual radius in the discrete elements modeling is set equal to one spatial step in the Lattice-Boltzmann discretization (Δx), consequently, the space between each two grains contains at least one node of the Lattice-Boltzmann grid.

The simulated deposit is composed of 300 polydisperse grains, with maximum and minimum diameters of 0.4 and $0.8\,mm$ respectively. Periodic conditions are used in the horizontal direction with a period length of $14.4mm$. The resulting average deposit height is about $8.8mm$. The unit weight and kinematic viscosity of water are taken as $\gamma_w = 10kN/m^3$ and $\nu = 10^{-6}m^2$ respectively while the unit weight of solid grains γ_s is set to $26kN/m^3$. The grains are first deposited under gravity then placed into a water column of the same section and of larger height and subjected to an upward water flow. The Lattice-Boltzmann discretization in the horizontal direction is $400\Delta x$, so that the smallest grain diameter is discretized into about $11\Delta x$.

Starting from its classical expression, the hydraulic gradient could be written as $i = \frac{\gamma'}{\gamma_w}\frac{\Delta pS}{W'}$. where γ' is the submerged unit weight of the soil, Δp is the pressure drop between the lower and upper horizontal surfaces of the deposit, S and W' are the horizontal section and the submerged weight of the deposit respectively. The product ΔpS is the resultant of external pressures applied to the deposit. With increasing Δp, the quicksand phenomenon triggers when the resultant of external pressures equals the submerged weight of the deposit i.e. $\Delta pS = W'$, therefore the critical hydraulic gradient is $i_c = \frac{\gamma'}{\gamma_w}$ and the applied hydraulic gradient could be written in terms of the critical hydraulic gradient as $i = i_c\frac{\Delta pS}{W'}$. As S and W' are fixed (characteristics of the deposit), it results that in order to impose a fraction of the critical hydraulic gradient, the only parameter to select is the pressure drop Δp.

5.1 Flow under constant hydraulic gradients

The deposit is subjected to an upward flow by imposing a hydraulic gradient. The hydraulic gradient is varied gradually from very low values up to values close to the critical gradient. It is found that for low values of the gradient ($i \leqslant 0,97i_c$) no uplift of the deposit is observed. For ($i \geqslant 0,97i_c$) the uplift is observed but in different ways depending on the applied hydraulic gradient. Figure 4 shows the deposit evolution over time for three applied hydraulic gradients $i = 0,97i_c$, $i = i_c$ and $i = 1,1i_c$.

These snapshots show that quicksand occurs in a similar manner for gradients $i \geqslant i_c$, in fact the deposit is fully raised initially, but for a low gradient ($i = i_c$) it loosens quickly while for a high gradient it may be raised like a shutter. This can be attributed to the high pressure applied at the bottom of the deposit which prevents loosening. Furthermore, it can be observed that the lifting is more quicker for the high gradient, since the grains reach the end of the column of water in a shorter time; $0.18s$ for $i = 1.1i_c$ against $0.18s$ for $i = i_c$. For the case $i = 0.97i_c$, the snapshots show that quicksand develops step by step ; first there is a grain rearrangement in some areas at the bottom of the deposit that allows the creation of large channels where there is no pressure drop (surrounded areas on the second snapshot). Accordingly, the hydraulic gradient in the area overlying the channel becomes larger. This increase in gradient initiates an uprising of this zone which leads to the loosening of the lower zone. This loosening grows progressively until the quicksand onset. It should be noted that in this case ($i = 0.97i_c$) the quicksand process is much slower than in the case with $i \geqslant i_c$ (in this case the total process time is $0.9s$), and the initial stage i.e. the grain rearrangement is the most time consuming stage.

5.2 Flow under constant volumetric flow rates

The deposit is subjected to an upward flow by imposing a controlled flow rate. The flow rate is incremented from zero to relatively high values gradually. i.e. it is increased only after a sufficient number of time steps. For small flow rates where the deposit remains stable the incrementation is then done after the establishment of the steady state under the previous flow rate. Figure 5 shows snapshots of the deposit for different flow rates. It may be noted that, depending on the behavior of the deposit, the flow rates could be classified as low, medium and high. For low flow rates, the deposit remains stable ($Q \leq 1.26 \times 10^{-5} m^3/s$ in our case). The medium flows induce a deposit dilation behavior ($1.26 \times 10^{-5} m^3/s \leq Q \leq 12.0 \times 10^{-5} m^3/s$ in our case). For the first flow rates causing a dilation, only a widening of some intergranular channels is observed as surrounded in the snapshot $Q = 1.32 \times 10^{-5} m^3/s$. Then, from a certain level of flow rate, the deposit becomes unstable, it is observed a development of unstable water pockets within the deposit which rise irregularly towards the surface. These pockets are larger for large flow rates. The high flow rates corresponds to the formation and the evolution of a continuous tunnel between the upstream and the downstream sides as well as sand boils, as shown in the snapshots $Q = 18 \times 10^{-5} m^3/s$ and $Q = 24 \times 10^{-5} m^3/s$.

For each value of the flow rate we measured the porosity as well as the resulting hydraulic gradient. For small flow rates where the deposit remains at rest, the porosity and the hydraulic gradient are measured after the steady state is established. However for high flow rates the deposit becomes unstable, the porosity and the hydraulic gradient are then taken as averages over a sufficient number of time steps. Figures 6 and 7 show the evolution of the average porosity and the average hydraulic gradient with the imposed flow rate respectively. In Fig. 7, the hydraulic gradient is normalized with respect to critical hydraulic gradient. Figure 6 shows that the porosity remains constant for the

low flow rates, it slightly decreases before increasing almost proportionally to the flow imposed. This indicates that the deposit can contract for the first flow rates that cause destabilization and after the destabilization the dilation is almost proportional to the flow imposed.

Figure 7 shows that for low flow rates the resulting hydraulic gradient is proportional the the imposed flow rate which is in good agreement with Darcy's law. This plot shows also that the hydraulic gradient remains in all cases less than the critical hydraulic gradient indicating that the engagement of instability prevents the increase of the hydraulic gradient. The curve indicates also that once the flow rate reaches the destabilization value ($Q = 1.32 \times 10^{-5} m^3/s$) the gradient evolution ceases to increase abruptly.

6 Concluding remarks

We investigated the quicksand instability using a coupled Lattice-Boltzmann-Discrete element hydromechanical model. Simulations of an upward fluid flow through granular deposits are performed for two cases namely under a gradually increased hydraulic gradient and under a gradually increased volumetric flow rate. In the first case i.e. under controlled hydraulic gradient, the simulations show that the quicksand condition is actually reached for a hydraulic gradient very close to the critical hydraulic gradient calculated from the global analysis of classical soil mechanics. The simulations point out moreover that the quicksand phenomenon could be produced locally under slightly lower gradients. In the second case i.e. under gradually increased volumetric flow rate, the simulations show that there are three levels of flow ; low flow rates that allow seepage without any destabilization, medium flow rates that cause expansion of the deposit to increase its permeability, such expansion is almost proportional to the flow imposed. And high flow rates which may cause the formation of continuous tunnel between the upstream and the downstream sides as well as sand boils. It is shown also that under the controlled flow rate condition the hydraulic gradient remains in all cases less than the critical hydraulic gradient.

REFERENCES

[1] Mansouri, M., El Youssoufi, M. S. and Nicot, F. Numerical simulation of the quicksand phenomenon by a 3D coupled Discrete Element - Lattice Boltzmann hydromechanical model. *Int. J. Num. Anal. Meth. Geomech.* (2017) **41(3)**:338–358.

[2] Cundall, P. and Strack O., A discrete numerical model for granular assemblies, *Geotechnique* (1979) **29(1)**:47–65.

[3] Luo L. S., Theory of the lattice Boltzmann method: Lattice Boltzmann models for nonideal gases, *Physical Review E* (2000); **62(4)** : 4982–4996.

[4] Bouzidi, M., Firdaouss, M., Lallemand, P. Momentum transfer of a Boltzmann-lattice fluid with boundaries, *Physics of Fluids* (2001) **13**:3452–3459.

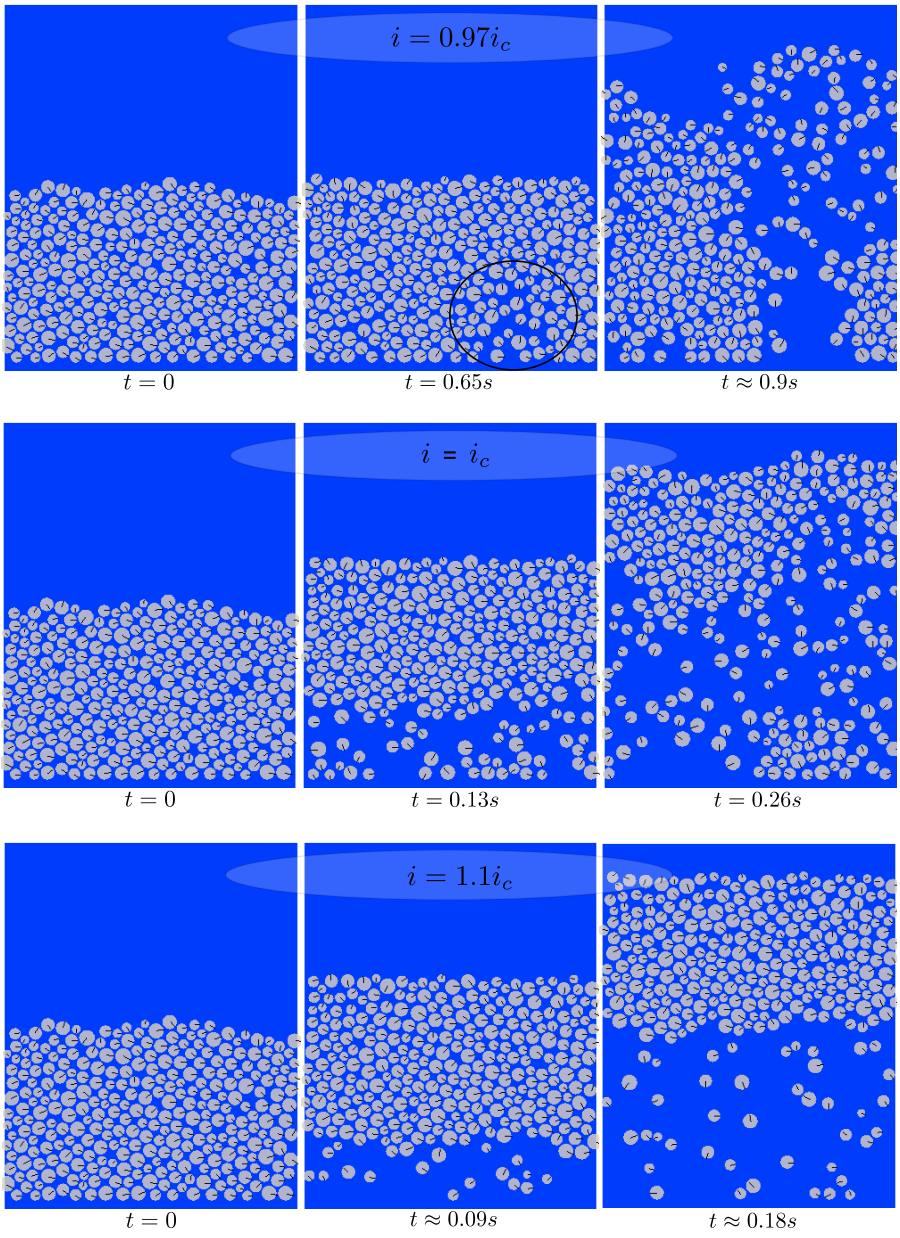

Figure 4: Snapshots in a chronological order, during the 2D simulation of the quicksand of a 300 grain deposit for imposed hydraulic gradients $i = 0.97i_c$, $i = i_c$ and $i = 1.1i_c$.

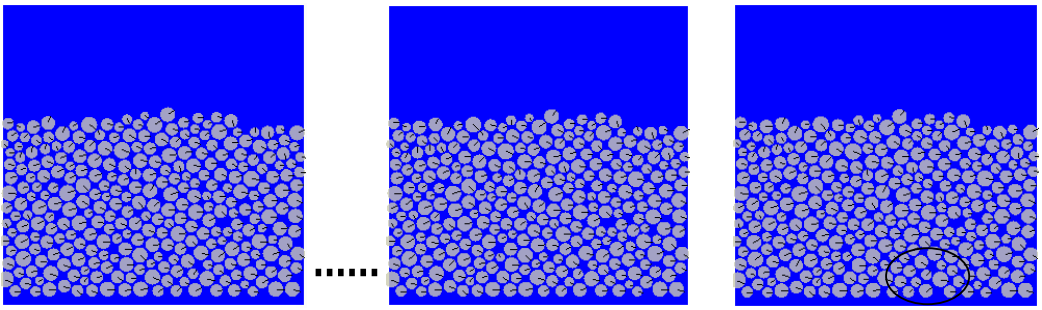

$Q = 0.0$ $Q = 1.26 \times 10^{-5} m^3/s$ $Q = 1.32 \times 10^{-5} m^3/s$

Snapshots of the deposit subjected to low flow rates

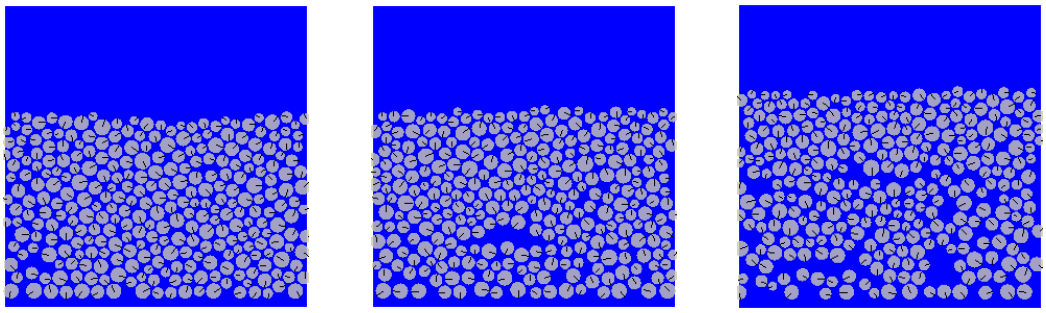

$Q = 2.4 \times 10^{-5} m^3/s$ $Q = 6.0 \times 10^{-5} m^3/s$ $Q = 12.0 \times 10^{-5} m^3/s$

Examples of snapshots of the deposit subjected to medium flow rates

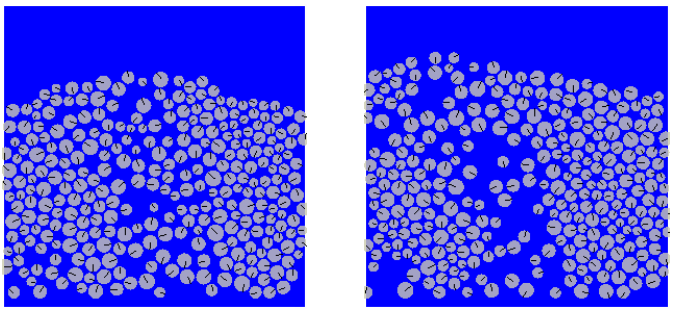

$Q = 18.0 \times 10^{-5} m^3/s$ $Q = 24.0 \times 10^{-5} m^3/s$

Examples of snapshots of the deposit subjected to high flow rates

Figure 5: Snapshots of the deposit subjected to an upward flow with different flow rates.

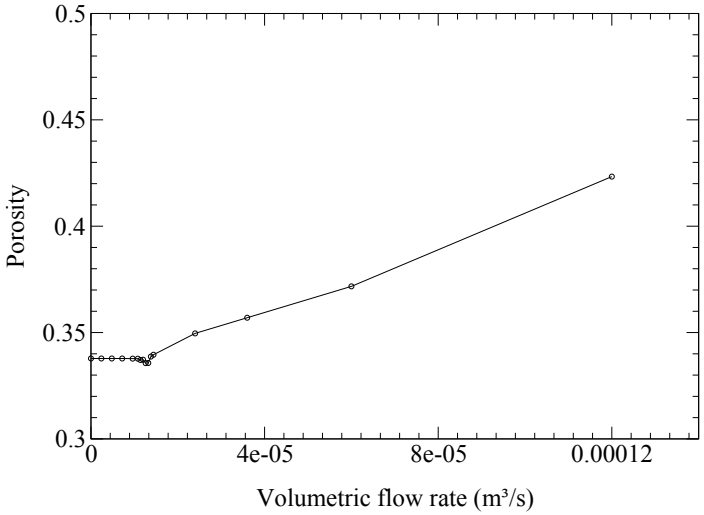

Figure 6: Evolution of the average porosity with the imposed flow rate

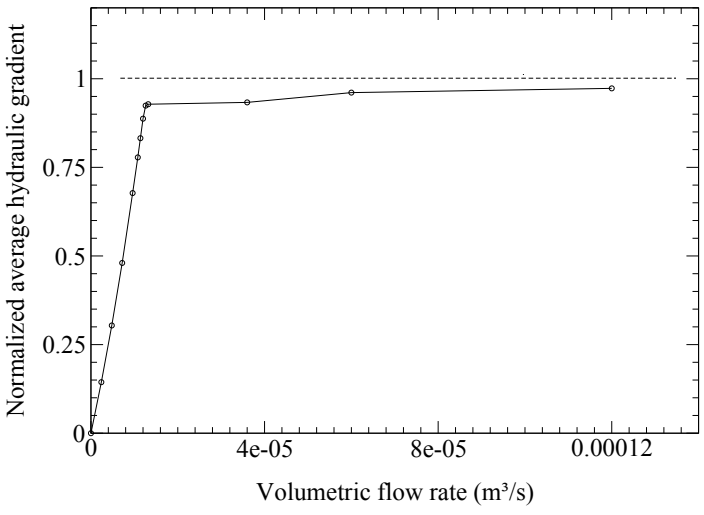

Figure 7: Evolution of the average hydraulic gradient with the imposed flow rate.